Hindawi Publishing Corporation
Mathematical Problems in Engineering
Volume 2013, Article ID 574072, 14 pages
http://dx.doi.org/10.1155/2013/574072

Research Article

Vibration Isolation Platform with Multiple Tuned Mass Dampers for Reaction Wheel on Satellites

Yao Zhang, Jingrui Zhang, and Guang Zhai

School of Aerospace Engineering, Beijing Institute of Technology, Beijing 100081, China

Correspondence should be addressed to Yao Zhang; zhangyao@bit.edu.cn

Received 18 March 2013; Revised 30 May 2013; Accepted 3 June 2013

Academic Editor: Rongni Yang

Vibration isolation is a direct and effective approach to improve the ultraprecise pointing capability of an imaging satellite. To have a good trade-off between the resonance amplitude and the high frequency attenuation for the original vibration isolation platform, a novel vibration isolation system for reaction wheel (RW), including a multistrut vibration isolation platform and multiple tuned mass dampers, is proposed. The first step constructs the integrated satellite dynamic model including the RWs and the vibration isolation systems, while the static and dynamic imbalances of the rotor and base movements are considered in the modeling process. The transmissibility matrix of the vibration isolation system is then obtained, and its frequency domain characteristics are described. The third part presents the application of the vibration isolation system for RWs. The effective attenuation of RW disturbances by the new vibration isolation system is illustrated, and its safety performance is also verified. Finally, using the reasonable parameters of the vibration isolation system, its performance on the satellite is testified by numerical simulations. The study shows that the novel vibration isolation system presented cannot only be successfully applied to a satellite but also improve the attitude stability.

1. Introduction

Recently, spacecraft with high pointing accuracy and stability gains increasing importance in space missions. For example, the Hubble Space Telescope (HST) requires the pointing stability to be less than 0.007 arcsecond within periods up to 24 hours [1]. The James Webb Space Telescope (JWST) needs the line of sight motion to be 4 milliarcseconds [2]. The Terrestrial Planet Finder Coronagraph (TPF-C) must also maintain the pointing accuracy to 4 milli-arcseconds in order to meet the minimum science requirements [3].

For this class of spacecraft, attitude control torques are usually provided by reaction wheels (RWs) which produce continuous torques to realize high precision pointing control and perform large angle slewing maneuvers. However, Masterson et al. [4] found that the RW can also produce tonal disturbances, and broadband noises when the wheel spins, due to the imbalance of the rotor, the imperfections in the spin bearings, motor disturbances and motor driven errors, thus making it one of the largest disturbance sources onboard the spacecraft. To mitigate these effects on the spacecraft pointing control, the vibration isolation technology is often used for the RW. HST used viscous fluid dampers called the D-Struts to attenuate the axial disturbances of the RWs [5]. The Defense Satellite Communications System III Spacecraft applied four damped stainless steel spring isolators supporting an RW to provide six degrees of freedom wheel isolation [6]. The Chandra X-ray Observatory employed a hexapod isolator at each of its six RWs to achieve multidimensional vibration isolation [7]. This passive vibration isolation platform will be employed in JWST as the first isolation stage [8]. Moreover, Kamesh et al. [9] designed a flexible platform consisting of folded continuous beams arranged in three dimensions to act as a mount for each fly wheel.

However, in designing the above-mentioned vibration isolation systems of RWs, the researchers ignored the dynamic characteristics of the RW. The RW should constantly adjust its speed to realize attitude stabilization or attitude maneuver. Its disturbance force is caused by the static imbalance of the rotor, whose amplitude is proportional to the square of the wheel speed, and whose frequency is the same as the wheel speed. Consequently, a resonance condition will occur when the wheel speed and the corner frequencies of the above-mentioned vibration isolation systems come close.

This resonance will cause more serious vibrations to the satellite, significantly influencing the image performance of the optical payload on the satellites. If the resonance amplitude is large enough, the vibration isolation system will lose the ability to transfer effective torques, causing rapid catastrophic attitude control system failure. A tuned mass damper (TMD) is a device mounted in structures to reduce the amplitude of mechanical vibrations, the application of which can prevent discomfort, damage, or outright structural failure. Therefore, it is frequently used in power transmission, automobiles, and buildings [10]. The achievements of the dynamic analysis and simulation method for the TMD are valuable. For example, Hoang et al. [11] have focused on optimal design of a TMD for a single degree of freedom structure and shown that for large mass ratios TMD becomes very effective in minimizing the primary structure response and robust against uncertainties in the parameters of the system. Li et al. [12] developed a single foot force model for the vertical component of walking-induced force and presented the optimal design parameters method for the multiple TMDs. For the dynamic analysis of space structures with multiple TMDs, Guo and Chen [13] presented the formulations of the reverberation matrix method. However, the previous dynamic models all ignored the base movements and the dynamic characteristics of the vibration source.

In addition, up to now, jitter performances of the spacecraft using the vibration isolation system for RWs have been predicted in some missions, such as the Space Interferometer Mission (SIM) [14], Terrestrial Planet Finder Coronagraph (TPF-C) [15], the GONES-N spacecraft [16], and Solar Dynamics observatory (SDO) [17]. In these literatures, the structures of spacecraft are all modeled by the finite-element method, with some using the vibration isolation system consisting of 6 decoupled second-order low-pass filters to approximate the effect of a passive fly wheel mount [18]. These accurate finite element models are necessary to predict the jitter performance of the spacecraft. However, the analysis using finite element models has some limitations. The spacecraft structure, for instance, should be well known, the dynamic coupling cannot be obtained, and the finite element model is not suitable for attitude controller designs based on the modern control theory.

This paper aims to design a new vibration isolation system for RW which cannot only satisfy the brace stiffness requirement but also reduce the resonance amplitude. The dynamic model of an integrated satellite system with RWs and the new vibration isolation system is constructed with Newton-Euler approach. The frequency domain characteristics of the vibration isolation system are described. Reasonable parameters of the vibration isolation system are employed to testify its performance on the satellite in numerical simulations.

2. Dynamics Model of the Integrated Satellite with RWs and Vibration Isolation System

2.1. Description of RW Disturbances. The present study only focuses on the rotor imbalance considered in the RW disturbances since the magnitudes of disturbances from motor errors and bearing imperfections are relatively small. The RW reference frames used in the modeling are shown in Figure 1 and are defined as follows:

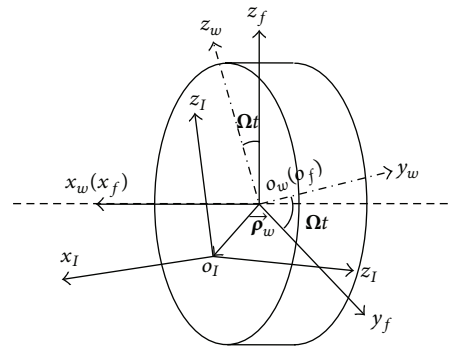

Figure 1: Reference frames.

(1) quasi-geometric body frame of the rotor: $\mathbf{f}_f(o_f x_f y_f z_f)$, whose origin is fixed at the geometric centre of the rotor, with its x-axis along the spin axis of rotor, and y and z axes in the rotating plane of the rotor perpendicular to x-axis. The axes do not rotate as the rotor does;

(2) geometric body frame of the rotor: $\mathbf{f}_w(o_w x_w y_w z_w)$, fixed to the rotor with its origin at the geometric centre, and its x-axis along the spin axis. In addition, $\mathbf{f}_w$ coincides with $\mathbf{f}_f$ in the initial state;

(3) principal axes of the inertia frame of the rotor: $\mathbf{f}_I(o_I x_I y_I z_I)$, fixed to the rotor with its origin at the centroid, its x-axis along the principal axis of the inertia in the spin axial direction. The vector $\boldsymbol{\rho}_w$ from o_w to o_I and the rotation angles μ and η from $\mathbf{f}_w$ to $\mathbf{f}_I$ represent the static and dynamic imbalances of the rotor, respectively.

For the unification of notations, we define $\mathbf{A}_{nm}$ as the coordinate transformation matrix from frame $\mathbf{f}_m$ to frame $\mathbf{f}_n$ and $\mathbf{r}_{nm}$ the vector from o_m to o_n. The static imbalance of the rotor can be expressed in frame $\mathbf{f}_w$ as $\boldsymbol{\rho}_w = [\gamma \ \ \xi \ \ \zeta]^T$, where γ, ξ, and ζ are three relatively small constants, showing the offset of the center of mass of the rotor from its spin axis. With high order small quantities ignored, the dynamic imbalance of the rotor can be expressed as

$$\begin{aligned}\mathbf{A}_{Iw} &= \mathbf{A}_y(\mu)\,\mathbf{A}_z(\eta)\\ &= \begin{bmatrix}\cos\mu & 0 & -\sin\mu\\ 0 & 1 & 0\\ \sin\mu & 0 & \cos\mu\end{bmatrix}\begin{bmatrix}\cos\eta & \sin\eta & 0\\ -\sin\eta & \cos\eta & 0\\ 0 & 0 & 1\end{bmatrix}\\ &\approx \begin{bmatrix}1 & \eta & -\mu\\ -\eta & 1 & 0\\ \mu & 0 & 1\end{bmatrix},\end{aligned} \tag{1}$$

where μ and η are small Euler angles from frame $\mathbf{f}_w$ to frame $\mathbf{f}_I$.

2.2. System Configuration and Reference Frames Definitions. In this research, the RW of a satellite is isolated separately, forming a combined system with the vibration isolation system. Figure 2 gives a schematic representation of the combined RW/vibration isolation system.

As for the platform part, a passive multistrut vibration isolation platform based on the Stewart platform is adopted. Multiple tuned mass dampers are installed on the payload platform to attenuate the resonant amplitude. Each strut of the platform includes an upper part, a lower part, a spring, and a damper connecting the two parts. The struts are connected to the payload platform by spherical joints and the base platform by universal joints. The moments of inertia of the struts are taken into account in the modeling process. To build a general dynamic model of an integrated satellite with RWs, we assume that there are L RWs, N struts of each vibration isolation platform, and H tuned mass dampers installed on the payload platform. Considering the convenience of the satellite modeling, this paper redivides the system into four parts as follows: each payload platform system, tuned mass dampers, struts, and the base platform system, where the payload platform system consists of a payload platform and a RW with rotor imbalances, and the base platform system includes all the base platforms and the satellite bus.

The reference frames used in the modeling are shown in Figure 3 and are defined as follows:

(1) inertial frame: $\mathbf{f}_e(o_e x_e y_e z_e)$, fixed in the inertial space;

(2) body frame of the satellite: $\mathbf{f}_b(o_b x_b y_b z_b)$, with its origin at the reference point of the satellite, and axes fixed in the satellite;

(3) body frame of the payload platform: $\mathbf{f}_p(o_p x_p y_p z_p)$, with its origin at the mass center of the payload platform, and axes fixed in the payload platform;

(4) body frame of the base platform: $\mathbf{f}_d(o_d x_d y_d z_d)$, with its origin at the mass center of the base platform, and axes fixed in the base platform;

(5) body frame of the hth tuned mass damper: $\mathbf{f}_{th}(o_{th} x_{th} y_{th} z_{th})$, with its origin at the mass center of the hth tuned mass damper, and axes fixed in the hth tuned mass damper. It is the same orientation as $\mathbf{f}_p(o_p x_p y_p z_p)$ in the initial state;

(6) lower frame of the ith strut: $\mathbf{f}_{di}(o_{di} x_{di} y_{di} z_{di})$, attached to the lower part of the ith strut with its origin at the connection point to the base platform, x-axis along the strut, y-axis along the rotating axis (axis fixed to the strut) of the universal joint, z-axis perpendicular to the x and y axes according to the right hand rule;

(7) upper frame of the ith strut: $\mathbf{f}_{ui}(o_{ui} x_{ui} y_{ui} z_{ui})$, attached to the upper part of the ith strut with its origin at the connection point to the payload platform. It is the same orientation as $\mathbf{f}_{di}(o_{di} x_{di} y_{di} z_{di})$ in the initial state.

In Figure 3, $\mathbf{t}$ is the position vector from the origin of the inertial frame to the mass center of the payload platform, and

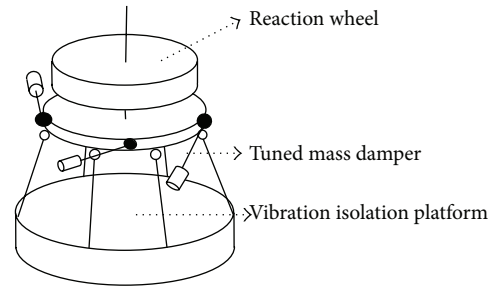

Figure 2: Combined RW/vibration isolation system configuration.

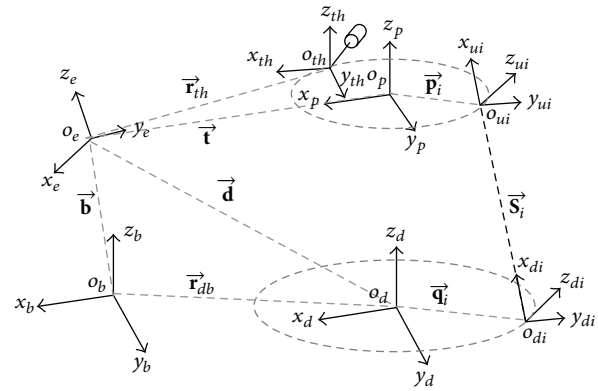

Figure 3: Reference frames (vibration isolation system part).

$\mathbf{d}$ is the position vector from the origin of the inertial frame to the mass center of the base platform. $\mathbf{r}_{th}$ is the position vector from the origin of the inertial frame to the mass center of the hth tuned mass damper. $\mathbf{p}_i$ is the vector from the mass center of the payload platform to its connection point. $\mathbf{q}_i$ is the vector from the mass center of the base platform to its connection point. $\mathbf{r}_{db}$ is the vector from the origin of $\mathbf{f}_b$ to the origin of $\mathbf{f}_d$. $\mathbf{S}_i$ is the vector of the ith strut (vector from the origin of frame $\mathbf{f}_{di}$ to the origin of frame $\mathbf{f}_{ui}$).

The modeling method adopted in this paper is based on the Newton-Euler approach employed by Dasgupta and Mruthyunjaya to derive the dynamic formulation of a Stewart platform [19]. Since the RW is introduced, the dynamic model of the payload platform system is similar to a spacecraft with a momentum exchange actuator. Therefore, the frame of the modeling process is as follows: firstly, establish the equations for the motion of the struts, the tuned mass dampers, each payload platform system, and the base platform system separately; then, combine those equations to form the dynamic formulation of the whole system. Particularly, it should be noticed that the motion of each strut is determined by the position and angular information of platforms, and that the forces and torques at joints are given by the dynamics of struts. In addition, the motion of each tuned mass damper is determined by the position and angular information of the payload platform, and that the forces and torques at joints are given by the dynamics of the tuned mass dampers.

2.3. Kinematics and Dynamics of Struts. Here and throughout, it is assumed that there are N struts in the combined

system. The ith strut vector $\mathbf{S}_i$ and its derivatives are defined as follows:

$$\begin{aligned}
\mathbf{S}_i &= \mathbf{t} + \mathbf{A}_{ep}\mathbf{p}_i - \mathbf{d} - \mathbf{A}_{eb}\mathbf{q}_i,\\
\dot{\mathbf{S}}_i &= \dot{\mathbf{t}} + \mathbf{A}_{ep}\boldsymbol{\omega}_p^{\times}\mathbf{p}_i - \dot{\mathbf{d}} - \mathbf{A}_{eb}\boldsymbol{\omega}_b^{\times}\mathbf{q}_i,\\
\ddot{\mathbf{S}}_i &= \ddot{\mathbf{t}} + \mathbf{A}_{ep}\dot{\boldsymbol{\omega}}_p^{\times}\mathbf{p}_i + \mathbf{A}_{ep}\boldsymbol{\omega}_p^{\times}\boldsymbol{\omega}_p^{\times}\mathbf{p}_i - \ddot{\mathbf{d}} - \mathbf{A}_{ed}\dot{\boldsymbol{\omega}}_d^{\times}\mathbf{q}_i\\
&\quad - \mathbf{A}_{ed}\boldsymbol{\omega}_d^{\times}\boldsymbol{\omega}_d^{\times}\mathbf{q}_i,
\end{aligned} \tag{2}$$

where $\boldsymbol{\omega}_p$ and $\boldsymbol{\omega}_d$ are the angular velocities of the payload and the base platform, respectively. The superscript "×" denotes the cross product matrix.

The strut length and the unit vector along the strut are given by

$$l_i = \left\|\mathbf{S}_i\right\|, \qquad \hat{\mathbf{s}}_i = \frac{\mathbf{S}_i}{l_i}. \tag{3}$$

The angular velocity and angular acceleration of the ith strut are obtained by

$$\begin{aligned}
\boldsymbol{\omega}_{li} &= \boldsymbol{\omega}_{li1} + \omega_{li2}\hat{\mathbf{s}}_i,\\
\boldsymbol{\varepsilon}_{li} &= \boldsymbol{\varepsilon}_{li1} + \varepsilon_{li2}\hat{\mathbf{s}}_i,
\end{aligned} \tag{4}$$

where $\boldsymbol{\omega}_{li1}$ and $\boldsymbol{\varepsilon}_{li1}$ are the angular velocity and angular acceleration perpendicular to the strut and $\omega_{li2}\hat{\mathbf{s}}_i$ and $\varepsilon_{li2}\hat{\mathbf{s}}_i$ are the components along the strut direction.

Consider

$$\begin{aligned}
\boldsymbol{\omega}_{li1} &= \frac{\hat{\mathbf{s}}_i^{\times}\dot{\mathbf{S}}_i}{l_i}, \qquad \omega_{li2} = -\frac{\left(\boldsymbol{\omega}_{li1}^T\mathbf{h}_i\right)}{\left(\hat{\mathbf{s}}_i^T\mathbf{h}_i\right)},\\
\boldsymbol{\varepsilon}_{li1} &= \frac{1}{l_i}\left[\hat{\mathbf{s}}_i^{\times}\ddot{\mathbf{S}}_i - 2\dot{l}_i\boldsymbol{\omega}_{li} + 2\dot{l}_i\omega_{li2}\hat{\mathbf{s}}_i - l_i\omega_{li2}\left(\hat{\mathbf{s}}_i^{\times}\boldsymbol{\omega}_{li1}\right)\right],\\
\varepsilon_{li2} &= \frac{\left[\left(\boldsymbol{\varepsilon}_{li1}^T\mathbf{k}_i\right)\left(\mathbf{k}_i^T\hat{\mathbf{s}}_i\right) + \left(\omega_{ki}\omega_{yi}\right)\left(\mathbf{k}_i^{\times}\mathbf{y}_i\right)^T\hat{\mathbf{s}}_i\right]}{\left[1 - \left(\mathbf{k}_i^T\hat{\mathbf{s}}_i\right)^2\right]}.
\end{aligned} \tag{5}$$

In the previous expressions, $\omega_{ki} = \boldsymbol{\omega}_{li}^T\mathbf{k}_i$ and $\omega_{yi} = \boldsymbol{\omega}_{li1}^T\mathbf{y}_i$. $\mathbf{k}_i$ is the unit vector along the fixed axis of the universal joint, which is known if the installation of the universal joint is determined. $\mathbf{y}_i$ is the unit vector along the moving axis of the universal joint. $\mathbf{h}_i$ is the normal vector of the plane formed by $\mathbf{k}_i$ and $\mathbf{y}_i$. Expressions of $\mathbf{y}_i$ and $\mathbf{h}_i$ are

$$\begin{aligned}
\mathbf{y}_i &= \frac{\left(\mathbf{k}_i^{\times}\hat{\mathbf{s}}_i\right)}{\left\|\mathbf{k}_i^{\times}\hat{\mathbf{s}}_i\right\|},\\
\mathbf{h}_i &= \mathbf{y}_i^{\times}\mathbf{k}_i.
\end{aligned} \tag{6}$$

Then, the sliding velocity and acceleration between the two parts of the strut are

$$\begin{aligned}
\dot{l}_i &= \hat{\mathbf{s}}_i^T\dot{\mathbf{S}}_i,\\
\ddot{l}_i &= \hat{\mathbf{s}}_i^T\ddot{\mathbf{S}}_i - \hat{\mathbf{s}}_i^T\left[\boldsymbol{\omega}_{li}^{\times}\boldsymbol{\omega}_{li}^{\times}\mathbf{S}_i\right].
\end{aligned} \tag{7}$$

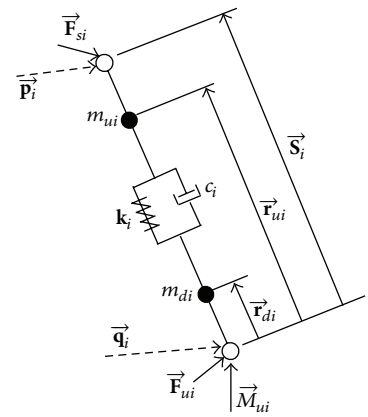

Figure 4: Details of one strut.

The linear accelerations of the centroids of the upper and lower parts of the strut can be expressed as

$$\begin{aligned}
\mathbf{a}_{ui} &= \mathbf{a}_{qi} + \boldsymbol{\varepsilon}_{li}^{\times}\mathbf{r}_{ui} + \boldsymbol{\omega}_{li}^{\times}\boldsymbol{\omega}_{li}^{\times}\mathbf{r}_{ui} + \ddot{l}_i\hat{\mathbf{s}}_i + 2\boldsymbol{\omega}_{li}^{\times}\dot{l}_i\hat{\mathbf{s}}_i,\\
\mathbf{a}_{di} &= \mathbf{a}_{qi} + \boldsymbol{\varepsilon}_{li}^{\times}\mathbf{r}_{di} + \boldsymbol{\omega}_{li}^{\times}\boldsymbol{\omega}_{li}^{\times}\mathbf{r}_{di},
\end{aligned} \tag{8}$$

where $\mathbf{a}_{qi} = \ddot{\mathbf{d}} + \mathbf{A}_{ed}\dot{\boldsymbol{\omega}}_d^{\times}\mathbf{q}_i + \mathbf{A}_{ed}\boldsymbol{\omega}_d^{\times}\boldsymbol{\omega}_d^{\times}\mathbf{q}_i$ is the linear acceleration of o_{di}, $\mathbf{r}_{ui}$ and $\mathbf{r}_{di}$ are the vectors from o_{di} to the centroids of the upper and the lower parts, respectively, and $\dot{l}_i$ and $\ddot{l}_i$ are the sliding velocity and sliding acceleration between the two parts.

The details of one strut are shown in Figure 4. Considering the moments acting on the strut in the inertial frame, Euler's equation for the whole strut can be obtained as follows:

$$\begin{aligned}
&\left(\mathbf{I}_{ui} + \mathbf{I}_{di}\right)\boldsymbol{\varepsilon}_{li} + \boldsymbol{\omega}_{li}^{\times}\left(\mathbf{I}_{ui} + \mathbf{I}_{di}\right)\boldsymbol{\omega}_{li}\\
&\quad = \mathbf{S}_i^{\times}\mathbf{F}_{si} + M_{ui}\mathbf{h}_i - c_{si}\left(\boldsymbol{\omega}_{li} - \mathbf{A}_{ep}\boldsymbol{\omega}_p\right)\\
&\qquad - c_{ui}\left(\boldsymbol{\omega}_{li} - \mathbf{A}_{ed}\boldsymbol{\omega}_d\right) - \left(m_{ui}\mathbf{r}_{ui} + m_{di}\mathbf{r}_{di}\right)^{\times}\mathbf{a}_{qi}.
\end{aligned} \tag{9}$$

Newton's equation for the whole strut is

$$m_{ui}\mathbf{a}_{ui} + m_{di}\mathbf{a}_{di} = \mathbf{F}_{si} + \mathbf{F}_{ui}, \tag{10}$$

where m_{ui} and m_{di} are the masses of the lower and upper parts of the ith strut, $\mathbf{I}_{ui}$ and $\mathbf{I}_{di}$ are moments of inertia of the lower and upper parts of the ith strut with respect to point o_{di} (expressed in the inertial frame), $\mathbf{F}_{si}$ and $\mathbf{F}_{ui}$ are the constrained forces at the spherical joint and the universal joint acting on the strut, respectively, $M_{ui}\mathbf{h}_i$ is the constrained torque at the universal joint acting on the strut, and c_{si} and c_{ui} are the coefficients of viscous friction in the spherical and universal joints, respectively.

Solving (9) and (10), we obtain

$$\begin{aligned}
M_{ui} &= \frac{\hat{\mathbf{s}}_i^T\mathbf{C}_i}{\left(\hat{\mathbf{s}}_i^T\mathbf{h}_i\right)},\\
\mathbf{F}_{si} &= \frac{X_i\hat{\mathbf{s}}_i - \left(\hat{\mathbf{s}}_i^{\times}\mathbf{C}_i - \hat{\mathbf{s}}_i^{\times}M_{ui}\mathbf{h}_i\right)}{l_i},\\
\mathbf{F}_{ui} &= m_{ui}\mathbf{a}_{ui} + m_{di}\mathbf{a}_{di} - \mathbf{F}_{si},
\end{aligned} \tag{11}$$

where

$$\begin{aligned}\mathbf{C}_i &= \left(\mathbf{I}_{ui}+\mathbf{I}_{di}\right)\boldsymbol{\varepsilon}_{li}+\boldsymbol{\omega}_{li}^{\times}\left(\mathbf{I}_{ui}+\mathbf{I}_{di}\right)\boldsymbol{\omega}_{li}+c_{si}\left(\boldsymbol{\omega}_{li}-\mathbf{A}_{ep}\boldsymbol{\omega}_p\right)\\&\quad+c_{ui}\left(\boldsymbol{\omega}_{li}-\mathbf{A}_{ed}\boldsymbol{\omega}_d\right)+\left(m_{ui}\mathbf{r}_{ui}+m_{di}\mathbf{r}_{di}\right)^{\times}\mathbf{a}_{qi},\\X_i &= \widehat{\mathbf{s}}_i^T\mathbf{F}_{si}=m_{ui}\widehat{\mathbf{s}}_i^T\mathbf{a}_{ui}+k_i\left(l_i-l_{i0}\right)+c_i\dot{l}_i,\end{aligned}\tag{12}$$

where k_i and c_i are the coefficients of stiffness and viscous damping of the ith strut, respectively, and l_{i0} is the nominal strut length.

2.4. Dynamic Equations for Tuned Mass Dampers. Here and throughout, it is assumed that there are H tuned mass dampers in the vibration isolation system. Taking o_{th} as the reference point, we can derive the dynamic equations of the hth tuned mass damper from theorems of moment and moment of momentum

$$\begin{aligned}&m_h\mathbf{A}_{pe}\ddot{\mathbf{r}}_{th}+\mathbf{C}_{ht}\mathbf{A}_{pe}\left(\dot{\mathbf{r}}_{th}-\dot{\mathbf{t}}-\mathbf{A}_{ep}\boldsymbol{\omega}_p^{\times}\mathbf{t}_h\right)\\&\qquad+\mathbf{K}_{ht}\mathbf{A}_{pe}\left(\mathbf{r}_{th}-\mathbf{t}-\mathbf{A}_{ep}\mathbf{t}_h\right)=\mathbf{0}_{3\times1},\\&\mathbf{A}_{pth}\left(\mathbf{I}_h\dot{\boldsymbol{\omega}}_{th}+\boldsymbol{\omega}_{th}^{\times}\mathbf{I}_h\boldsymbol{\omega}_{th}\right)\\&\qquad=-\left[\mathbf{K}_{hr}\left(\boldsymbol{\theta}_{th}-\boldsymbol{\theta}_p\right)+\mathbf{C}_{hr}\left(\mathbf{A}_{pth}\boldsymbol{\omega}_{th}-\boldsymbol{\omega}_p\right)\right],\end{aligned}\tag{13}$$

where m_h and $\mathbf{I}_h$ are the mass and moment of inertia of the hth tuned mass damper, respectively, and $\mathbf{t}_h$ represents the vector from the origin of $\mathbf{f}_p$ to the origin of $\mathbf{f}_{th}$, with $\boldsymbol{\omega}_{th}$ being the angular velocity of the hth tuned mass damper, $\boldsymbol{\theta}_{th}$ and $\boldsymbol{\theta}_p$ being the attitude angles of the hth tuned mass damper and the payload platform, respectively. In this paper, the tuned mass damper is regarded as a 6-dof vibration system. Therefore, each tuned mass damper not only has translational stiffness and damping coefficient matrices $\mathbf{K}_{ht}$ and $\mathbf{C}_{ht}$ but also contains rotational stiffness and damping coefficient matrices $\mathbf{K}_{hr}$ and $\mathbf{C}_{hr}$.

According to (13), the constrained forces and the constrained torque at the joint between the hth tuned mass damper and the payload platform can be solved as

$$\begin{aligned}\mathbf{F}_{th}&=\mathbf{C}_{ht}\mathbf{A}_{pe}\left(\dot{\mathbf{r}}_{th}-\dot{\mathbf{t}}-\mathbf{A}_{ep}\boldsymbol{\omega}_p^{\times}\mathbf{t}_h\right)\\&\quad+\mathbf{K}_{ht}\mathbf{A}_{pe}\left(\mathbf{r}_{th}-\mathbf{t}-\mathbf{A}_{ep}\mathbf{t}_h\right),\\\mathbf{T}_{th}&=\mathbf{K}_{hr}\Delta\boldsymbol{\theta}_{th}+\mathbf{C}_{hr}\left(\mathbf{A}_{pth}\boldsymbol{\omega}_{th}-\boldsymbol{\omega}_p\right)\\&\quad+\mathbf{t}_h^{\times}\left[\mathbf{C}_{ht}\mathbf{A}_{pe}\left(\dot{\mathbf{r}}_{th}-\dot{\mathbf{t}}-\mathbf{A}_{ep}\boldsymbol{\omega}_p^{\times}\mathbf{t}_h\right)\right.\\&\qquad\left.+\mathbf{K}_{ht}\mathbf{A}_{pe}\left(\mathbf{r}_{th}-\mathbf{t}-\mathbf{A}_{ep}\mathbf{t}_h\right)\right],\end{aligned}\tag{14}$$

where $\Delta\boldsymbol{\theta}_{th}=\boldsymbol{\theta}_{th}-\boldsymbol{\theta}_p$.

2.5. Dynamic Equations for Each Payload Platform System. Because of the rotor imbalance, the position of the centroid of the payload platform system changes incessantly during the operation of the RW. For the convenience of modeling, we take o_p as the reference point and establish the absolute angular momentum of the system.

We assume that there are L RWs, and that each RW has one matching vibration isolation system. In this section, the dynamic equations for the jth payload platform system are derived. For the simplification of these equations, we do not write the subscript j in the later discussion, and the number of RWs can be selected by some space missions.

Omitting some derivation processes, here we present the absolute linear and angular momentums of the jth rotor directly as follows:

$$\begin{aligned}\mathbf{p}_w&=m_w\left(\mathbf{v}_p+\boldsymbol{\omega}_p^{\times}\mathbf{r}_{fp}\right)-m_w\mathbf{A}_{pw}\boldsymbol{\rho}_w^{\times}\mathbf{A}_{wp}\left(\boldsymbol{\omega}_p+\mathbf{A}_{pf}\boldsymbol{\Omega}\right),\\\mathbf{h}_w^{o_p}&=m_w\mathbf{r}_{fp}^{\times}\left(\mathbf{v}_p+\boldsymbol{\omega}_p^{\times}\mathbf{r}_{fp}+\boldsymbol{\omega}_p^{\times}\mathbf{A}_{pw}\boldsymbol{\rho}_w+\mathbf{A}_{pf}\boldsymbol{\Omega}^{\times}\mathbf{A}_{fp}\mathbf{A}_{pw}\boldsymbol{\rho}_w\right)\\&\quad+m_w\mathbf{A}_{pw}\boldsymbol{\rho}_w^{\times}\mathbf{A}_{wp}\left(\mathbf{v}_p+\boldsymbol{\omega}_p^{\times}\mathbf{r}_{fp}\right)+\mathbf{A}_{pw}\mathbf{I}_{ww}^{o_f}\mathbf{A}_{wp}\\&\quad\times\left(\boldsymbol{\omega}_p+\mathbf{A}_{pf}\boldsymbol{\Omega}\right),\end{aligned}\tag{15}$$

where m_w is the mass of the rotor and $\mathbf{I}_{ww}^{o_f}=\mathbf{A}_{wI}\mathbf{I}_{wI}^{o_I}\mathbf{A}_{Iw}+m_w(\boldsymbol{\rho}_w^T\boldsymbol{\rho}_w\mathbf{E}_3-\boldsymbol{\rho}_w\boldsymbol{\rho}_w^T)$ is the moment of inertia of the rotor with respect to its geometric centre (in frame $\mathbf{f}_w$). $\mathbf{I}_{wI}^{o_I}=\mathrm{diag}(\mathbf{I}_{wIx}\ \ \mathbf{I}_{wIy}\ \ \mathbf{I}_{wIz})$ is the moment of inertia of the rotor with respect to its centroid (in frame $\mathbf{f}_I$); $\boldsymbol{\Omega}_j$ represents the angular velocity of the rotor with respect to the payload platform, which has the same expressions in frames $\mathbf{f}_f$ and $\mathbf{f}_w$; $\mathbf{v}_p$ represents the absolute linear velocity of point o_p.

The absolute linear and angular momentums of the payload platform are

$$\begin{aligned}\mathbf{p}_p&=m_{pp}\mathbf{v}_p,\\\mathbf{h}_p^{o_p}&=\mathbf{I}_{pp}^{o_p}\boldsymbol{\omega}_p,\end{aligned}\tag{16}$$

where m_{pp} is the mass of the payload platform and $\mathbf{I}_{pp}^{o_p}$ is the moment of inertia of the payload platform (in frame $\mathbf{f}_p$).

Thus, we can get the absolute linear and angular momentums of the payload platform system as follows:

$$\begin{aligned}\mathbf{p}&=\mathbf{p}_p+\mathbf{p}_w,\\\mathbf{h}^{o_p}&=\mathbf{h}_p^{o_p}+\mathbf{h}_w^{o_p}.\end{aligned}\tag{17}$$

By using the theorems of momentum and moment of momentum, the dynamic equations of the payload platform system can be written as

$$\begin{aligned}m_{pp}\left(\dot{\mathbf{v}}_p+\boldsymbol{\omega}_p^{\times}\mathbf{v}_p\right)&=\mathbf{F}+\mathbf{F}_{a1}+\mathbf{F}_{a2}+\mathbf{F}_d,\\\mathbf{I}_{pp}^{o_p}\dot{\boldsymbol{\omega}}_p+\boldsymbol{\omega}_p^{\times}\mathbf{I}_{\mathrm{pp}}^{o_p}\boldsymbol{\omega}_p&=\mathbf{T}+\mathbf{T}_{a1}+\mathbf{T}_{a2}+\mathbf{T}_c+\mathbf{T}_{d1}+\mathbf{T}_{d2},\end{aligned}\tag{18}$$

where $\mathbf{F}_{a1}$ is the coupling force acted on the payload platform by RWs, $\mathbf{F}_{a2}$ the additional coupling force due to the rotor static imbalance, and $\mathbf{F}_d$ the disturbance force generated by the rotor static imbalance, composed of Coriolis, tangential, and centrifugal forces due to the change of position of the centroid of the payload platform system. $\mathbf{F}$ is the sum of

forces at the spherical joints and tuned mass dampers joints acting on the payload platform. $\mathbf{T}_{a1}$ is the coupling torque acted on the payload platform by RWs. $\mathbf{T}_{a2}$ is the additional coupling torque due to the rotor static imbalance. $\mathbf{T}_c$ is the control torque generated by RWs. $\mathbf{T}_{d1}$ is the disturbance torque generated by the rotor static imbalance. $\mathbf{T}_{d2}$ is the disturbance torque generated by the rotor dynamic imbalance. $\mathbf{T}$ is the sum of torques at the spherical joints and the tuned mass dampers joints acting on the payload platform. The expressions of these previous symbols are

$$\begin{aligned}
\mathbf{F}_{a1} &= -m_w\left(\dot{\mathbf{v}}_p + \boldsymbol{\omega}_p^{\times}\mathbf{v}_p + \dot{\boldsymbol{\omega}}_p^{\times}\mathbf{r}_{fp} + \boldsymbol{\omega}_p^{\times}\boldsymbol{\omega}_p^{\times}\mathbf{r}_{fp}\right),\\
\mathbf{F}_{a2} &= -m_w\left(\dot{\boldsymbol{\omega}}_p^{\times} + \boldsymbol{\omega}_p^{\times}\boldsymbol{\omega}_p^{\times}\right)\mathbf{A}_{pw}\boldsymbol{\rho}_w,\\
\mathbf{F}_d &= -2m_w\boldsymbol{\omega}_p^{\times}\mathbf{A}_{pw}\boldsymbol{\Omega}^{\times}\boldsymbol{\rho}_w - m_w\mathbf{A}_{pw}\left(\dot{\boldsymbol{\Omega}}^{\times} + \boldsymbol{\Omega}^{\times}\boldsymbol{\Omega}^{\times}\right)\boldsymbol{\rho}_w,\\
\mathbf{F} &= -\sum_{i=1}^{N}\mathbf{A}_{pe}\mathbf{F}_{si} + \sum_{h=1}^{H}\mathbf{F}_{th},\\
\mathbf{T}_{a1} &= -\left(\mathbf{A}_{pw}\mathbf{I}_{ww}^{o_f}\mathbf{A}_{wp} - m_w\mathbf{r}_{fp}^{\times}\mathbf{r}_{fp}^{\times}\right)\dot{\boldsymbol{\omega}}_p\\
&\quad - \boldsymbol{\omega}_p^{\times}\left(\mathbf{A}_{pw}\mathbf{I}_{ww}^{o_f}\mathbf{A}_{wp} - m_w\mathbf{r}_{fp}^{\times}\mathbf{r}_{fp}^{\times}\right)\boldsymbol{\omega}_p\\
&\quad - m_w\mathbf{r}_{fp}^{\times}\left(\dot{\mathbf{v}}_p + \boldsymbol{\omega}_p^{\times}\mathbf{v}_p\right),\\
\mathbf{T}_{a2} &= m_w\left[\mathbf{r}_{fp}^{\times}\mathbf{A}_{pw}\boldsymbol{\rho}_w^{\times}\mathbf{A}_{wp} + \left(\mathbf{r}_{fp}^{\times}\mathbf{A}_{pw}\boldsymbol{\rho}_w^{\times}\mathbf{A}_{wp}\right)^T\right]\dot{\boldsymbol{\omega}}_p\\
&\quad + m_w\boldsymbol{\omega}_p^{\times}\left[\mathbf{r}_{fp}^{\times}\mathbf{A}_{pw}\boldsymbol{\rho}_w^{\times}\mathbf{A}_{wp} + \left(\mathbf{r}_{fp}^{\times}\mathbf{A}_{pw}\boldsymbol{\rho}_w^{\times}\mathbf{A}_{wp}\right)^T\right]\boldsymbol{\omega}_p\\
&\quad - m_w\mathbf{A}_{pw}\boldsymbol{\rho}_w^{\times}\mathbf{A}_{wp}\left(\dot{\mathbf{v}}_p + \boldsymbol{\omega}_p^{\times}\mathbf{v}_p\right),\\
\mathbf{T}_c &= -\mathbf{A}_{pw}\mathbf{I}_{ww}^{o_f}\dot{\boldsymbol{\Omega}} - \boldsymbol{\omega}_p^{\times}\mathbf{A}_{pw}\mathbf{I}_{ww}^{o_f}\boldsymbol{\Omega},\\
\mathbf{T}_{d1} &= \mathbf{r}_{fp}^{\times}\mathbf{F}_d,\\
\mathbf{T}_{d2} &= \mathbf{A}_{pw}\left[\mathbf{I}_{ww}^{o_f}\boldsymbol{\Omega}^{\times} + \left(\mathbf{I}_{ww}^{o_f}\boldsymbol{\Omega}^{\times}\right)^T\right]\left(\mathbf{A}_{wp}\boldsymbol{\omega}_p + \boldsymbol{\Omega}\right),\\
\mathbf{T} &= -\sum_{i=1}^{N}\mathbf{p}_i^{\times}\mathbf{A}_{pe}\mathbf{F}_{si} + \sum_{i=1}^{N}c_{si}\left(\mathbf{A}_{pe}\boldsymbol{\omega}_{li} - \boldsymbol{\omega}_p\right) + \sum_{h=1}^{H}\mathbf{T}_{th}.
\end{aligned} \tag{19}$$

2.6. Dynamic Equations for the Base Platform System. Taking o_b as the reference point, we can derive the dynamic equations of the base platform system from theorems of moment and moment of momentum

$$\begin{aligned}
m_b\left(\dot{\mathbf{v}}_b + \boldsymbol{\omega}_b^{\times}\mathbf{v}_b + \dot{\boldsymbol{\omega}}_b^{\times}\boldsymbol{\rho}_b + \boldsymbol{\omega}_b^{\times}\boldsymbol{\omega}_b^{\times}\boldsymbol{\rho}_b\right) &= \mathbf{F}' + \mathbf{F}_{\text{ext}},\\
\mathbf{I}_b\dot{\boldsymbol{\omega}}_b + \boldsymbol{\omega}_b^{\times}\mathbf{I}_b\boldsymbol{\omega}_b + m_b\boldsymbol{\rho}_b^{\times}\left(\dot{\mathbf{v}}_b + \boldsymbol{\omega}_b^{\times}\mathbf{v}_b\right) &= \mathbf{T}' + \mathbf{T}_{\text{ext}},
\end{aligned} \tag{20}$$

where m_b and $\mathbf{I}_b$ are the mass and the moment of inertia of the base platform system, respectively, and $\mathbf{v}_b$ represents the absolute velocity of point o_b, with $\boldsymbol{\omega}_b$ being the angular velocity of the base platform system, $\mathbf{F}_{\text{ext}}$ and $\mathbf{T}_{\text{ext}}$ the external disturbing force and torque acting on the satellite being, respectively, $\boldsymbol{\rho}_b$ being the vector from o_b to the centroid of the base platform system, and $\mathbf{F}'$ and $\mathbf{T}'$ being the sum of forces and the sum of torques at the universal joints acting on the base platform system. They can be shown as follows:

$$\begin{aligned}
\mathbf{F}' &= -\sum_{i=1}^{N}\mathbf{A}_{be}\mathbf{F}_{ui},\\
\mathbf{T}' &= -\sum_{i=1}^{N}\left(\mathbf{A}_{bd}\mathbf{q}_i + \mathbf{r}_{db}\right)^{\times}\mathbf{A}_{be}\mathbf{F}_{ui} + \sum_{i=1}^{N}c_{ui}\left(\mathbf{A}_{be}\boldsymbol{\omega}_{li} - \boldsymbol{\omega}_b\right)\\
&\quad - \sum_{i=1}^{N}\mathbf{A}_{be}M_{ui}\mathbf{h}_i.
\end{aligned} \tag{21}$$

Equation (21) only describes the sum of forces and the sum of torques on one combined system including the RW and the vibration isolation platform. If L RWs are employed on a satellite, it means that there are L combined systems. $\mathbf{F}'$ and $\mathbf{T}'$ can be rewritten as follows:

$$\begin{aligned}
\mathbf{F}' &= -\mathbf{A}_{be}\left(\sum_{j=1}^{L}\sum_{i=1}^{N}\mathbf{F}_{uji}\right),\\
\mathbf{T}' &= \sum_{j=1}^{L}\left[\sum_{i=1}^{N}\left(\mathbf{A}_{bdj}\mathbf{q}_{ij} + \mathbf{r}_{djb}\right)^{\times}\mathbf{A}_{be}\mathbf{F}_{uji}\right.\\
&\quad \left. + \sum_{i=1}^{N}c_{uji}\left(\mathbf{A}_{bje}\boldsymbol{\omega}_{lji} - \boldsymbol{\omega}_b\right) - \sum_{i=1}^{N}\mathbf{A}_{be}M_{uji}\mathbf{h}_{ji}\right].
\end{aligned} \tag{22}$$

In the previous equations, j means the jth RW. The expression of each symbol including j is the same as that in the only one combined system state. The transformation matrix $\mathbf{A}_{bdj}$, the vector from the mass center of the jth base platform to its connection point $\mathbf{q}_{ij}$, and the vector from the origin of $\mathbf{f}_b$ to the origin of the jth body frame of the jth base platform $\mathbf{r}_{djb}$ will be determined by the installation of the combined systems.

Hence, (13), (18), and (20) form the complete dynamic equations of the integrated satellite with the RWs and the new vibration isolation system.

As mentioned above, kinematics of the struts are all expressed by $\mathbf{d}$ and $\boldsymbol{\omega}_d$; however, in the dynamic equations of the base platform system, $\mathbf{v}_b$ and $\boldsymbol{\omega}_b$ are used to describe the motion information of a satellite. In order to make the integrated satellite dynamic equations solvable, the relationship between the kinematics of the struts and the motion information of a satellite should be derived. As we know, $\boldsymbol{\omega}_q = \boldsymbol{\omega}_b$. $\mathbf{d}$ and its derivatives can be rewritten as

$$\begin{aligned}
\mathbf{d} &= \mathbf{r}_b + \mathbf{A}_{eb}\mathbf{r}_{db},\\
\dot{\mathbf{d}} &= \mathbf{A}_{eb}\left(\mathbf{v}_b + \boldsymbol{\omega}_b^{\times}\mathbf{r}_{db}\right),\\
\ddot{\mathbf{d}} &= \mathbf{A}_{eb}\left(\dot{\mathbf{v}}_b + \boldsymbol{\omega}_b^{\times}\mathbf{v}_b + \dot{\boldsymbol{\omega}}_b^{\times}\mathbf{r}_{db} + \boldsymbol{\omega}_b^{\times}\boldsymbol{\omega}_b^{\times}\mathbf{r}_{db}\right).
\end{aligned} \tag{23}$$

3. Frequency Domain Characteristics Analysis of the New Vibration Isolation System

3.1. Derivation of the Transmissibility Matrix. Transmissibility is the amount of force or motion transferred across the isolation interface as a function of frequency. For the vibration isolation system presented in this paper, the disturbance acting on the payload platform has 6-DOF input, the satellite bus has 6-DOF output, and the transmissibility from the payload platform to the satellite bus is a 6×6 matrix, which is named as transmissibility matrix [20]. To derive the transmissibility matrix of the vibration isolation platform with multiple tuned mass dampers, the following assumptions are made.

The platform configuration does not change because the amplitude of vibration is small. The transformation matrix $\mathbf{A}_{bd}$ from the satellite body frame to the base platform frame is an identity matrix according to the position relation between the satellite and the vibration isolation platform. The transformation matrices $\mathbf{A}_{ep}$ and $\mathbf{A}_{eb}$ from the payload and base platform frames, respectively, to the inertial frame can be seen as the identity matrices, and the square of angular velocities can be ignored because both the attitude angles and the angular velocities are small under the attitude stabilization control. Based on this small angle assumption, $\boldsymbol{\omega}_{th} - \boldsymbol{\omega}_p$ can be rewritten as $\dot{\boldsymbol{\theta}}_{th} - \dot{\boldsymbol{\theta}}_p$. Since the influence of strut's moment of inertia and mass on the transfer function of the vibration isolation platform is small, they can be ignored. o_b is the same as the centroid of the base platform system; therefore $\boldsymbol{\rho}_b$ is a zero vector.

Based on the previous assumptions, the simplified dynamic equations of the integrated satellite are

$$\begin{aligned} &m_h\ddot{\mathbf{r}}_{th} + \mathbf{C}_{ht}\left(\dot{\mathbf{r}}_{th} - \dot{\mathbf{t}} + \mathbf{t}_h^{\times}\boldsymbol{\theta}_p\right) \\ &\quad + \mathbf{K}_{ht}\left(\mathbf{r}_{th} - \mathbf{t} - \mathbf{t}_h - \boldsymbol{\theta}_p^{\times}\mathbf{t}_h\right) = \mathbf{0}_{3\times 1}, \\ &\mathbf{I}_h\ddot{\boldsymbol{\theta}}_{th} = -\left[\mathbf{K}_{hr}\left(\boldsymbol{\theta}_{th} - \boldsymbol{\theta}_p\right) + \mathbf{C}_{hr}\left(\dot{\boldsymbol{\theta}}_{th} - \dot{\boldsymbol{\theta}}_p\right)\right], \end{aligned} \tag{24}$$

$$\begin{aligned} m_p\ddot{\mathbf{t}} &= -\sum_{i=1}^{N}\mathbf{F}_{si} + \sum_{h=1}^{H}\mathbf{F}_{th} + \mathbf{F}_d, \\ \mathbf{I}_p\ddot{\boldsymbol{\theta}}_p &= -\sum_{i=1}^{N}\mathbf{p}_i^{\times}\mathbf{F}_{si} + \sum_{h=1}^{H}\mathbf{T}_{th} + \mathbf{T}_d, \end{aligned} \tag{25}$$

$$\begin{aligned} m_b\ddot{\mathbf{b}} &= -\sum_{i=1}^{N}\mathbf{F}_{ui}, \\ \mathbf{I}_b\ddot{\boldsymbol{\theta}}_b &= -\sum_{i=1}^{N}\left(\mathbf{q}_i + \mathbf{r}_{db}\right)^{\times}\mathbf{F}_{ui}, \end{aligned} \tag{26}$$

where $\boldsymbol{\theta}_b$ is the attitude angles of the satellite and m_p and $\mathbf{I}_p$ are the mass and moment of inertia of the payload platform system, respectively. $m_p = m_{pp} + m_w$, $\mathbf{I}_p = \mathbf{I}_{pp}^{o_p} + (\mathbf{A}_{pw}\mathbf{I}_{ww}^{o_f}\mathbf{A}_{wp} - m_w\mathbf{r}_{fp}^{\times}\mathbf{r}_{fp}^{\times})$. $\mathbf{F}_d$ and $\mathbf{T}_d$ are the sum of disturbance forces and sum of torques caused by RWs, respectively.

Denote $\mathbf{x}_h = \begin{bmatrix} \mathbf{r}_{th} - \mathbf{t}_h \\ \boldsymbol{\theta}_{th} \end{bmatrix}$, $\mathbf{x}_p = \begin{bmatrix} \mathbf{t} \\ \boldsymbol{\theta}_p \end{bmatrix}$, $\mathbf{x}_d = \begin{bmatrix} \mathbf{b} \\ \boldsymbol{\theta}_b \end{bmatrix}$, and (24) can be rewritten as

$$\overline{\mathbf{M}}_h\ddot{\mathbf{x}}_h - \overline{\mathbf{C}}_{hp}\dot{\mathbf{x}}_p + \overline{\mathbf{C}}_h\dot{\mathbf{x}}_h - \overline{\mathbf{K}}_{hp}\mathbf{x}_p + \overline{\mathbf{K}}_h\mathbf{x}_h = \mathbf{0}_{6\times 1}, \tag{27}$$

where

$$\begin{aligned} \overline{\mathbf{M}}_h &= \begin{bmatrix} m_h\mathbf{E}_3 & \\ & \mathbf{I}_h \end{bmatrix}, \qquad \overline{\mathbf{C}}_{hp} = \begin{bmatrix} \mathbf{C}_{ht} & -\mathbf{C}_{ht}\mathbf{t}_h^{\times} \\ & \mathbf{C}_{hr} \end{bmatrix}, \\ \overline{\mathbf{C}}_h &= \begin{bmatrix} \mathbf{C}_{ht} & \\ & \mathbf{C}_{hr} \end{bmatrix}, \\ \overline{\mathbf{K}}_{hp} &= \begin{bmatrix} \mathbf{K}_{ht} & -\mathbf{K}_{ht}\mathbf{t}_h^{\times} \\ & \mathbf{K}_{hr} \end{bmatrix}, \qquad \overline{\mathbf{K}}_h = \begin{bmatrix} \mathbf{K}_{ht} & \\ & \mathbf{K}_{hr} \end{bmatrix}. \end{aligned} \tag{28}$$

Based on the previous assumption of small attitude angles, the expression of $\mathbf{F}_{th}$ and that of $\mathbf{T}_{th}$ (see (14)) are presented as

$$\overline{\mathbf{F}}_{th} = -\overline{\mathbf{C}}_{hpp}\dot{\mathbf{x}}_p + \overline{\mathbf{C}}_{hp}^T\dot{\mathbf{x}}_h - \overline{\mathbf{K}}_{hpp}\mathbf{x}_p + \overline{\mathbf{K}}_{hp}^T\mathbf{x}_h, \tag{29}$$

where

$$\begin{aligned} \overline{\mathbf{F}}_{th} &= \begin{bmatrix} \mathbf{F}_{th} \\ \mathbf{M}_{th} \end{bmatrix}, \qquad \overline{\mathbf{C}}_{hpp} = \begin{bmatrix} \mathbf{C}_{ht} & -\mathbf{C}_{ht}\mathbf{t}_h^{\times} \\ \mathbf{t}_h^{\times}\mathbf{C}_{ht} & \mathbf{C}_{hr} - \mathbf{t}_h^{\times}\mathbf{C}_{ht}\mathbf{t}_h^{\times} \end{bmatrix}, \\ \overline{\mathbf{K}}_{hpp} &= \begin{bmatrix} \mathbf{K}_{ht} & -\mathbf{K}_{ht}\mathbf{t}_h^{\times} \\ \mathbf{t}_h^{\times}\mathbf{K}_{ht} & \mathbf{K}_{hr} - \mathbf{t}_h^{\times}\mathbf{K}_{ht}\mathbf{t}_h^{\times} \end{bmatrix}. \end{aligned} \tag{30}$$

With the two-parameter isolator, the constraint force at the spherical joint acting on the upper part $\mathbf{F}_{si}$ is described as

$$\begin{aligned} \mathbf{F}_{si} &= k_i\hat{s}_i\hat{s}_i^T\mathbf{t} - k_i\hat{s}_i\hat{s}_i^T\mathbf{p}_i^{\times}\boldsymbol{\theta}_p - k_i\hat{s}_i\hat{s}_i^T\mathbf{b} \\ &\quad + k_i\hat{s}_i\hat{s}_i^T\left(\mathbf{q}_i + \mathbf{r}_{db}\right)^{\times}\boldsymbol{\theta}_b + c_i\hat{s}_i\hat{s}_i^T\dot{\mathbf{t}} - c_i\hat{s}_i\hat{s}_i^T\mathbf{p}_i^{\times}\dot{\boldsymbol{\theta}}_p \\ &\quad - c_i\hat{s}_i\hat{s}_i^T\dot{\mathbf{b}} + c_i\hat{s}_i\hat{s}_i^T\left(\mathbf{q}_i + \mathbf{r}_{db}\right)^{\times}\dot{\boldsymbol{\theta}}_b. \end{aligned} \tag{31}$$

Denote $\mathbf{x} = [\mathbf{x}_p^T \ \mathbf{x}_d^T \ \mathbf{x}_h^T]^T$, and $\mathbf{J}_i = [\hat{s}_i\hat{s}_i^T \ -\hat{s}_i\hat{s}_i^T\mathbf{p}_i^{\times} \ -\hat{s}_i\hat{s}_i^T \ \hat{s}_i\hat{s}_i^T(\mathbf{q}_i + \mathbf{r}_{db})^{\times} \ \mathbf{0}_{3\times(h\times 6)}]$.

Equation (31) can be rewritten as

$$\mathbf{F}_{si} = k_i\mathbf{J}_i\mathbf{x} + c_i\mathbf{J}_i\dot{\mathbf{x}}. \tag{32}$$

Equations (24)–(26) can be rewritten as

$$\overline{\mathbf{M}}\ddot{\mathbf{x}} + \overline{\mathbf{C}}\dot{\mathbf{x}} + \overline{\mathbf{K}}\mathbf{x} = \overline{\mathbf{U}}, \tag{33}$$

where

$$\mathbf{M} = \operatorname{diag}\left(\left[m_p\mathbf{E}_3 \;\; \mathbf{I}_p \;\; m_b\mathbf{E}_3 \;\; \mathbf{I}_b \;\; \overline{\mathbf{M}}_h\right]\right),$$

$$\overline{\mathbf{U}} = \begin{bmatrix} \mathbf{E}_6 \\ \mathbf{0}_{(1+h)\times 6} \end{bmatrix} \begin{bmatrix} \mathbf{F}_d \\ \mathbf{T}_d \end{bmatrix},$$

$$\overline{\mathbf{C}} = \sum_{i=1}^{N} c_i \begin{bmatrix} \mathbf{J}_i \\ \mathbf{p}_i^{\times}\mathbf{J}_i \\ -\mathbf{J}_i \\ -\left(\mathbf{q}_i + \mathbf{r}_{db}\right)^{\times}\mathbf{J}_i \\ \mathbf{0}_{(h\times 6)\times[12+(h\times 6)]} \end{bmatrix} + \begin{bmatrix} \overline{\mathbf{C}}_{1pp} + \cdots + \overline{\mathbf{C}}_{hpp} & \mathbf{0}_6 & -\overline{\mathbf{C}}_{hp}^{T} \\ \mathbf{0}_6 & \mathbf{0}_6 & \\ -\overline{\mathbf{C}}_{hp} & & \overline{\mathbf{C}}_{\mathbf{h}} \end{bmatrix}, \tag{34}$$

$$\overline{\mathbf{K}} = \sum_{i=1}^{N} k_i \begin{bmatrix} \mathbf{J}_i \\ \mathbf{p}_i^{\times}\mathbf{J}_i \\ -\mathbf{J}_i \\ -\left(\mathbf{q}_i + \mathbf{r}_{db}\right)^{\times}\mathbf{J}_i \\ \mathbf{0}_{(h\times 6)\times[12+(h\times 6)]} \end{bmatrix} + \begin{bmatrix} \overline{\mathbf{K}}_{1pp} + \cdots + \overline{\mathbf{K}}_{hpp} & \mathbf{0}_6 & -\overline{\mathbf{K}}_{hp}^{T} \\ \mathbf{0}_6 & \mathbf{0}_6 & \\ -\overline{\mathbf{K}}_{hp} & & \overline{\mathbf{K}}_1 \end{bmatrix},$$

where $\mathbf{E}_n$ is the $n \times n$ identity matrix and $\mathbf{0}_n$ is the $n \times n$ zero matrix.

The force and torque propagated into the satellite can be rewritten as

$$\overline{\mathbf{F}}_e = \overline{\mathbf{C}}_e\dot{\mathbf{x}} + \overline{\mathbf{K}}_e\mathbf{x}, \tag{35}$$

where

$$\overline{\mathbf{C}}_e = \sum_{i=1}^{N} c_i \begin{bmatrix} \mathbf{J}_i \\ \left(\mathbf{q}_i + \mathbf{r}_{db}\right)^{\times}\mathbf{J}_i \\ \mathbf{0}_{[6+(h\times 6)]\times[12+(h\times 6)]} \end{bmatrix},$$

$$\overline{\mathbf{K}}_e = \sum_{i=1}^{N} k_i \begin{bmatrix} \mathbf{J}_i \\ \left(\mathbf{q}_i + \mathbf{r}_{db}\right)^{\times}\mathbf{J}_i \\ \mathbf{0}_{[6+(h\times 6)]\times[12+(h\times 6)]} \end{bmatrix}. \tag{36}$$

Denote $\mathbf{X} = \left[\begin{smallmatrix} \mathbf{x} \\ \dot{\mathbf{x}} \end{smallmatrix}\right]$, and (33) and (35) can be described by the state equation as

$$\dot{\mathbf{X}} = \mathbf{A}\mathbf{X} + \mathbf{B}\mathbf{u},$$
$$\mathbf{Y} = \mathbf{C}_z\mathbf{X} + \mathbf{D}\mathbf{u}, \tag{37}$$

where

$$\mathbf{Y} = \overline{\mathbf{F}}_e, \qquad \mathbf{u} = \begin{bmatrix} \mathbf{F}_d \\ \mathbf{T}_d \end{bmatrix}, \qquad \mathbf{A} = \begin{bmatrix} \mathbf{0}_{12+(h\times 6)} & \mathbf{E}_{12+(h\times 6)} \\ -\overline{\mathbf{M}}^{-1}\overline{\mathbf{K}} & -\overline{\mathbf{M}}^{-1}\overline{\mathbf{C}} \end{bmatrix},$$

$$\mathbf{B} = \begin{bmatrix} \mathbf{0}_{[12+(h\times 6)]\times 6} \\ \overline{\mathbf{M}}^{-1}\begin{bmatrix} \mathbf{E}_6 \\ \mathbf{0}_{[6+(h\times 6)]\times 6} \end{bmatrix} \end{bmatrix}, \qquad \mathbf{C}_z = \left[\overline{\mathbf{K}}_e \;\; \overline{\mathbf{C}}_e\right],$$

$$\mathbf{D} = \mathbf{0}_6. \tag{38}$$

Therefore, the transmissibility matrix of the vibration isolation platform with multiple tuned mass dampers can be obtained by

$$\mathbf{G}(s) = \mathbf{C}(s\mathbf{E} - \mathbf{A})^{-1}\mathbf{B} + \mathbf{D}. \tag{39}$$

3.2. Analysis of the Frequency Domain. To isolate the disturbances induced by the RW for six DOF, a matching vibration isolation system is adopted. Figure 5 gives a schematic representation of this combined system.

The disturbances of the RW are propagated through the vibration isolation system to the satellite bus. Therefore, for each combined system, the transmissibility matrix from the RW to the satellite bus can be obtained by (39). The frequency response curve of each transfer function in transmissibility matrix can be drawn, and all of these frequency response curves can be illustrated by a matrix form figure, as shown in Figure 6. It means that the six-DOF RW disturbances can be propagated through this transmissibility matrix to yield the predicted six-DOF base force and torque.

From Figure 6, it can be clearly seen that the z-translation or "bounce" model and the z-rotation or "torsional" model are independent due to the symmetry of the platform, while the motion in the x direction is coupled with that in the θ_y direction, and the motion in the y direction is coupled with that in the θ_x direction. The curve of the transmissibility frequency response function in the x-x direction is the same as that in the y-y direction. In addition, there is the same characteristic as mentioned above in the θ_x-θ_x direction and the θ_y-θ_y direction. These characteristics depend on the symmetry of the Stewart platform.

3.3. Application of the Vibration Isolation System. To realize the attitude stabilization control and pointing ultraprecisely, four RWs (the mass of each RW is 9 kg) are adopted. The effective torque which is below 2 Hz and caused by RWs to the satellite for completing the attitude stabilization control must not be influenced. Moreover, the disturbances must be attenuated by more than 90% at frequencies above 100 Hz, and the resonance amplitude should be as small as possible.

Based on the previous requirements, we should design four identical vibration isolation systems to be installed between each RW and the satellite bus. The diameter of each vibration isolation platform is 150 mm, the length of each strut is 183.7 mm, and the height of each vibration isolation platform is 106 mm. The mass and the moment of inertia of each strut are

$$m_{ui} = 0.1\,\text{kg}, \qquad m_{di} = 0.2\,\text{kg},$$

$$\mathbf{I}_{ui} = \begin{bmatrix} 1.7\times 10^{-4} & 0 & 0 \\ 0 & 4.885\times 10^{-3} & 0 \\ 0 & 0 & 4.885\times 10^{-3} \end{bmatrix}\ \text{kg}\cdot\text{m}^2,$$

$$\mathbf{I}_{di} = \begin{bmatrix} 9.87\times 10^{-4} & 0 & 0 \\ 0 & 1.7449\times 10^{-2} & 0 \\ 0 & 0 & 1.7449\times 10^{-2} \end{bmatrix}\ \text{kg}\cdot\text{m}^2. \tag{40}$$

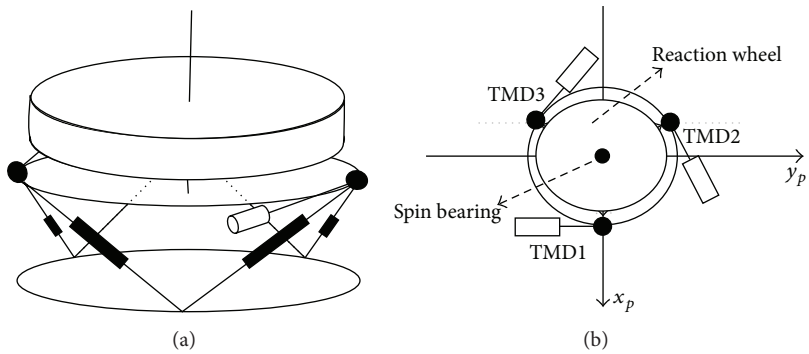

Figure 5: Schematic representation of one combined system.

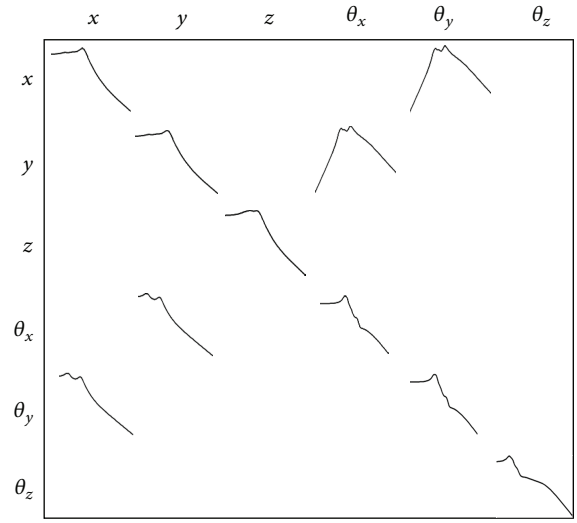

Figure 6: 6 by 6 frequency response curves of the transmissibility matrix for the vibration isolation system.

The stiffness coefficient and the damping coefficient of each strut are selected as 100000 N/m and 130 N·s/m, respectively. The corner frequencies obtained are within the interval 12.4 Hz~23.3 Hz.

To reduce the resonance amplitude of the vibration isolation platform, we use three tuned mass dampers installed on the payload platform. The parameters of the three tuned mass dampers can be obtained by "fminimax" function in MATLAB. The mass and the moment of inertia of three tuned mass dampers are as follows:

$$\begin{aligned} &m_1 = 0.15\,\text{kg}, \qquad m_2 = 0.26\,\text{kg}, \\ &m_3 = 0.31\,\text{kg}, \\ &\mathbf{I}_1 = \text{diag}\left(\left[0.022 \quad 0.0198 \quad 0.0297\right]\right)\ \text{kg}\cdot\text{m}^2, \\ &\mathbf{I}_2 = \text{diag}\left(\left[0.0248 \quad 0.0223 \quad 0.0335\right]\right)\ \text{kg}\cdot\text{m}^2, \\ &\mathbf{I}_3 = \text{diag}\left(\left[0.0321 \quad 0.0289 \quad 0.0434\right]\right)\ \text{kg}\cdot\text{m}^2. \end{aligned} \tag{41}$$

The position vectors of the tuned mass dampers are

$$\begin{aligned} &\mathbf{t}_1 = \left[0.15 \quad 0 \quad 0\right]^T \text{m}, \qquad \mathbf{t}_2 = \left[-0.075 \quad 0.075\sqrt{3} \quad 0\right]^T \text{m}, \\ &\mathbf{t}_3 = \left[-0.075 \quad -0.075\sqrt{3} \quad 0\right]^T \text{m}. \end{aligned} \tag{42}$$

The translational and rotational stiffness coefficient matrices are

$$\begin{aligned} &\mathbf{K}_{1t} = \text{diag}\left(\left[1713.3 \quad 1713.3 \quad 3104.6\right]\right)\ \text{N/m}, \\ &\mathbf{K}_{1r} = \text{diag}\left(\left[8.5663 \quad 8.5663 \quad 38.3328\right]\right)\ \text{N/m}, \\ &\mathbf{K}_{2t} = \text{diag}\left(\left[6673 \quad 6673 \quad 12092\right]\right)\ \text{N/m}, \\ &\mathbf{K}_{2r} = \text{diag}\left(\left[33.3652 \quad 33.3652 \quad 149.3043\right]\right)\ \text{N/m}, \\ &\mathbf{K}_{3t} = \text{diag}\left(\left[16094 \quad 16094 \quad 29165\right]\right)\ \text{N/m}, \\ &\mathbf{K}_{3r} = \text{diag}\left(\left[53.6474 \quad 53.6474 \quad 240.064\right]\right)\ \text{N/m}. \end{aligned} \tag{43}$$

The translational and rotational damping coefficient matrices are

$$\begin{aligned} &\mathbf{C}_{1t} = \text{diag}\left(\left[35.61 \quad 35.61 \quad 47.94\right]\right)\ \text{N}\cdot\text{s/m}, \\ &\mathbf{C}_{1r} = \text{diag}\left(\left[1.7805 \quad 1.7805 \quad 3.7665\right]\right)\ \text{N}\cdot\text{s/m}, \\ &\mathbf{C}_{2t} = \text{diag}\left(\left[108.68 \quad 108.68 \quad 146.30\right]\right)\ \text{N}\cdot\text{s/m}, \\ &\mathbf{C}_{2r} = \text{diag}\left(\left[5.434 \quad 5.434 \quad 11.495\right]\right)\ \text{N}\cdot\text{s/m}, \\ &\mathbf{C}_{3t} = \text{diag}\left(\left[152.17 \quad 152.17 \quad 204.85\right]\right)\ \text{N}\cdot\text{s/m}, \\ &\mathbf{C}_{3r} = \text{diag}\left(\left[7.609 \quad 7.609 \quad 16.095\right]\right)\ \text{N}\cdot\text{s/m}. \end{aligned} \tag{44}$$

With the substitution of the previous parameters into the transfer functions of the vibration isolation system, the frequency response curves can be drawn as shown in Figure 7, where the corner frequencies are within the interval [6.40 22.5] Hz, and more than 24 dB (94%) disturbances are attenuated at frequencies above 100 Hz. The maximal resonance amplitude is 5.31 dB (184%), which can well meet the engineering requirements. Therefore, for the vibration

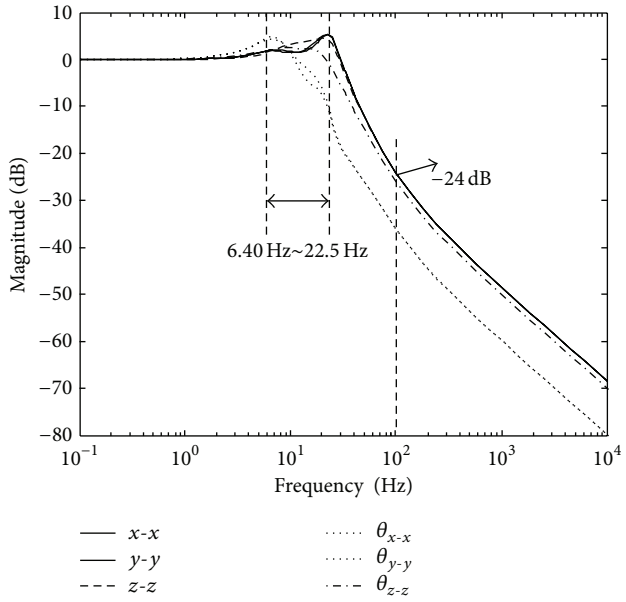

Figure 7: Transmissibility curves of the vibration isolation platform with three tuned mass dampers.

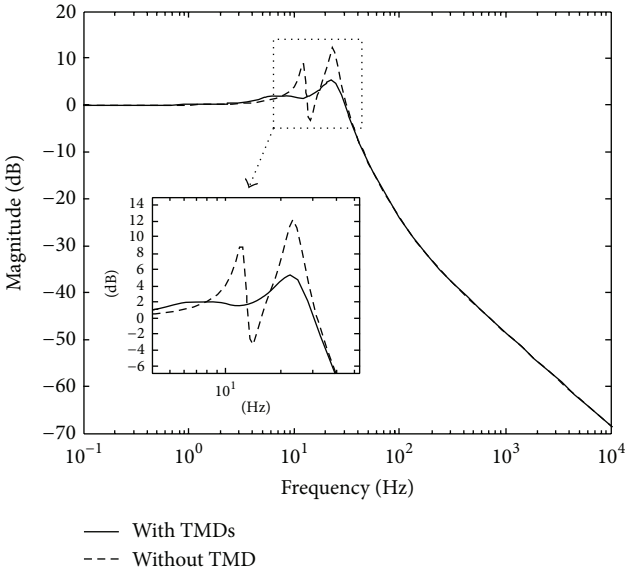

Figure 8: Transmissibility curves in the x-x direction.

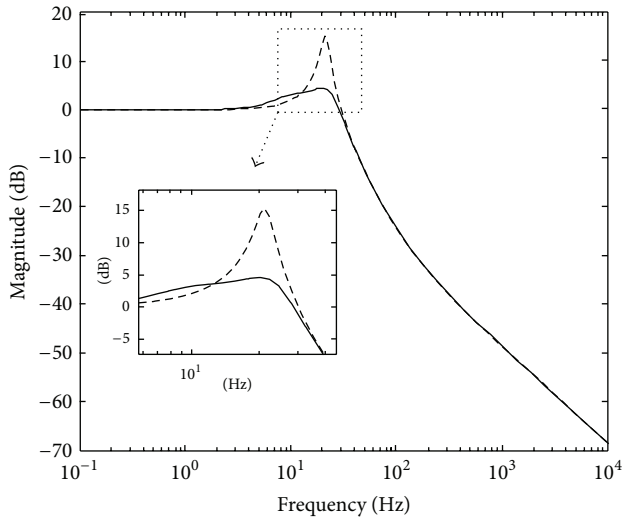

Figure 9: Transmissibility curves in the z-z direction.

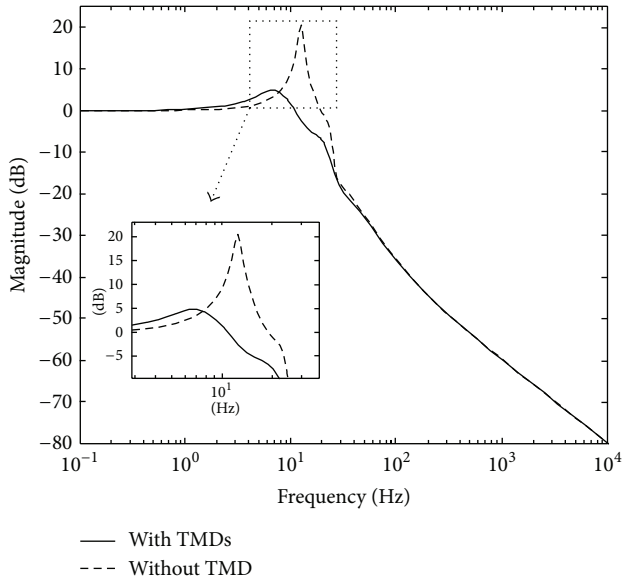

Figure 10: Transmissibility curves in the θ_x-θ_x direction.

isolation system with three tuned mass dampers, it is verified that the parameters selected are reasonable and this system can satisfy the previous requirements with the frequency domain method.

Furthermore, to demonstrate the competitive advantages of this new vibration isolation system, we draw the frequency response curves of the vibration isolation platform without tuned mass dampers as shown in Figures 8, 9, 10, and 11. Because of the symmetry of the vibration isolation system, the curve of the frequency response in the x-x direction is the same as that in the y-y direction. Furthermore, there is the same characteristic as the previous one in the θ_x-θ_x direction and the θ_y-θ_y direction. Therefore, we only draw the transmissibility curves in the x-x, z-z, θ_x-θ_x, and θ_z-θ_z directions.

To make the comparison clearer, the data of the resonance amplitude are displayed in Table 1.

Table 1 reveals that the resonance amplitude is greatly attenuated by using the tuned mass dampers. In addition, when the three tuned mass dampers are employed on the vibration isolation platform, the corner frequencies and the high frequency attenuation of the original vibration isolation platform do not change, which means that the new vibration isolation system has a good trade-off between the resonance amplitude and the high frequency attenuation.

Table 1: Resonance amplitude comparison in different directions.

	x-x direction	z-z direction	θ_x-θ_x direction	θ_z-θ_z direction
Resonance amplitude (original vibration isolation platform)	12.2 dB (4.07)	15.3 dB (5.82)	20.5 dB (10.60)	19.5 dB (9.44)
Resonance amplitude (new vibration isolation system)	5.31 dB (1.84)	4.59 dB (1.70)	4.85 dB (1.75)	2.55 dB (1.34)

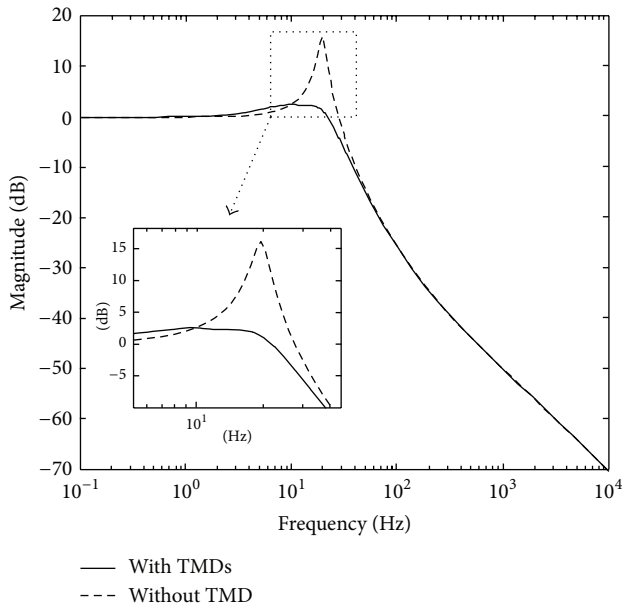

Figure 11: Transmissibility curves in the θ_z-θ_z direction.

4. Numerical Simulations

According to the combined system (RW and new vibration isolation system) dynamic model, the effects of the vibration isolation system have been described by a numerical simulation. The static and dynamic imbalance parameters of the RW are presumed as about 1.36 g·cm and 17 g·cm^2, respectively. To verify the advantage of the vibration isolation system on the resonance frequency, we select the speed of the RW as $1.25\pi t$, which can provide an effect torque of 0.125 Nm. When the stiffness coefficient and the damping coefficient of each strut are selected as 100000 N/m and 200 N·s/m, the disturbances attenuation curves with and without the vibration isolation system designed in this paper are shown in Figure 12.

Figure 12 clearly shows that the new vibration isolation system can attenuate the disturbances to a great extent. Then, we draw the comparison curves of disturbances attenuation with only the original vibration isolation platform and those with the new vibration isolation system as shown in Figure 13.

In Figure 13, when the original vibration isolation platform is used, the disturbance torque and disturbance force can reach 0.05 Nm and 0.4 N at the resonance frequency, respectively. The amplitude of these disturbances can be attenuated by using the tuned mass dampers in comparison with the previous status.

In order to obtain larger high frequency attenuation for the vibration isolation platform, the damping coefficient of each strut should be selected as smaller than 200 N·s/m. To further verify the validity of the new vibration isolation system, we select the damping coefficient of each strut as 130 N·s/m and draw the comparison curves of disturbances attenuation as displayed in Figure 14.

In Figure 14, when the speed of the RW crosses the resonance frequency, the vibration isolation platform with tuned mass dampers can work well, and the disturbance torque and disturbance force are 0.03 Nm and 0.25 N at resonance frequency, respectively. But for original vibration isolation platform, when the speed of the RW crosses the resonance frequency, the amplitudes of the disturbance force and disturbance torque always increase. These disturbances can cause rapid catastrophic failure. Therefore, it is evident that the tuned mass dampers cannot only attenuate the resonance amplitude but also ensure the security of the satellite system.

Based on the integrated satellite dynamic model with four combined systems, the attitude angular velocities of the integrated satellite can be simulated. From [21, 22], a PID controller is used to realize the three-axis stabilization. The parameters of PID controller K_p, K_i, and K_d can be obtained as 200, 0.1 and 2500, respectively. In this paper, the three initial attitude angles are all chosen as 1.5°. The four initial speeds of the RWs are all chosen as [3000 3000 3000 − 5196.2] rpm. The rotor motor, gimbal motor, attitude measurement, and the external disturbing torque acting on the satellite are ignored.

The mass and the moment of inertia of the satellite can be selected the same as those in [23],

$$m_b = 1000\,\text{kg}, \qquad \mathbf{I}_b = \begin{bmatrix} 1100 & -20 & -10 \\ -20 & 900 & -15 \\ -10 & -15 & 800 \end{bmatrix} \text{kg} \cdot \text{m}^2. \quad (45)$$

It can be seen from Figure 15 that the attitude angular velocities can converge well to their equilibriums, and the response time is appropriate. The simulation results (see Figure 16) of the speeds of RWs show that the RWs work normally and can provide sufficient torques to realize the attitude stabilization control. All the simulation results indicate that the selected parameters of the vibration isolation system are reasonable, by which the satellite can realize attitude stabilization.

When the satellite has no vibration isolation system for each RW, the maximal vibration amplitude of the attitude angular velocities is 6×10^{-6} rad/s, as shown in Figure 15(a). When the vibration isolation platform with tuned mass

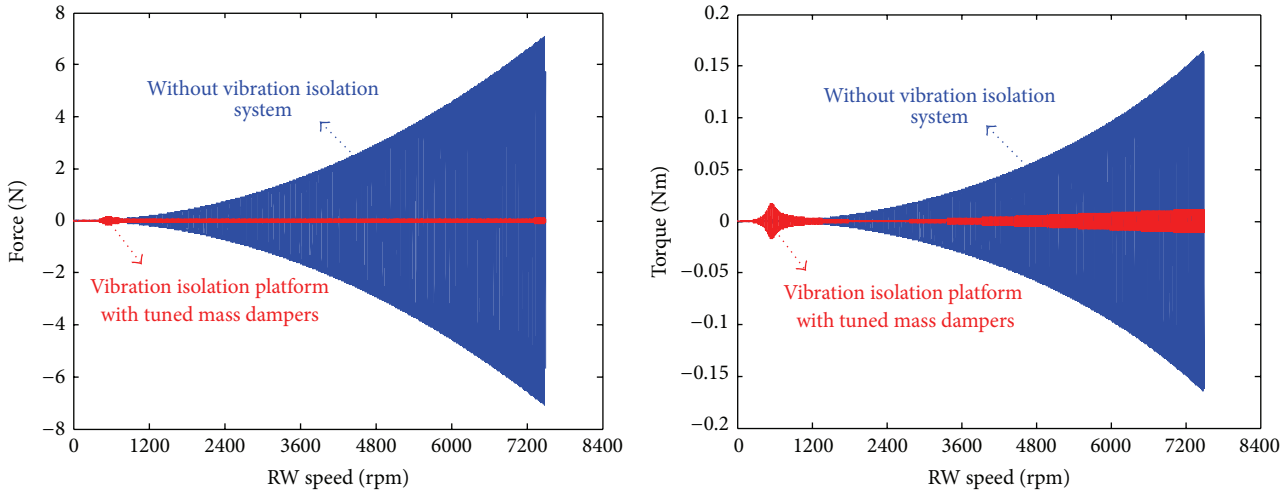

(a) (b)

Figure 12: Disturbance attenuation curves in x-x and θ_x-θ_x directions.

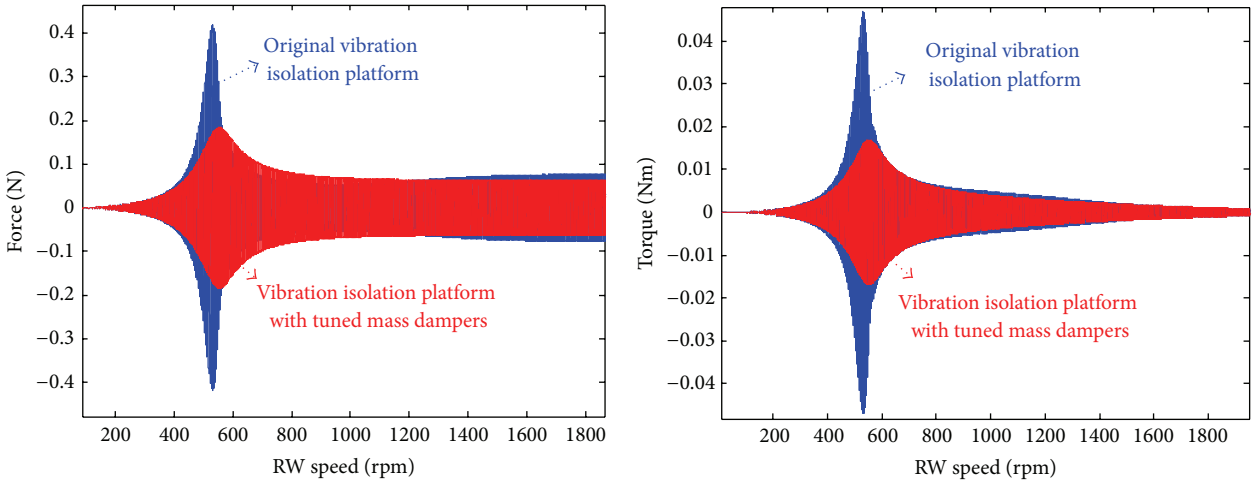

(a) (b)

Figure 13: Comparison curves of disturbances attenuation when the damping coefficient is 200 N·s/m.

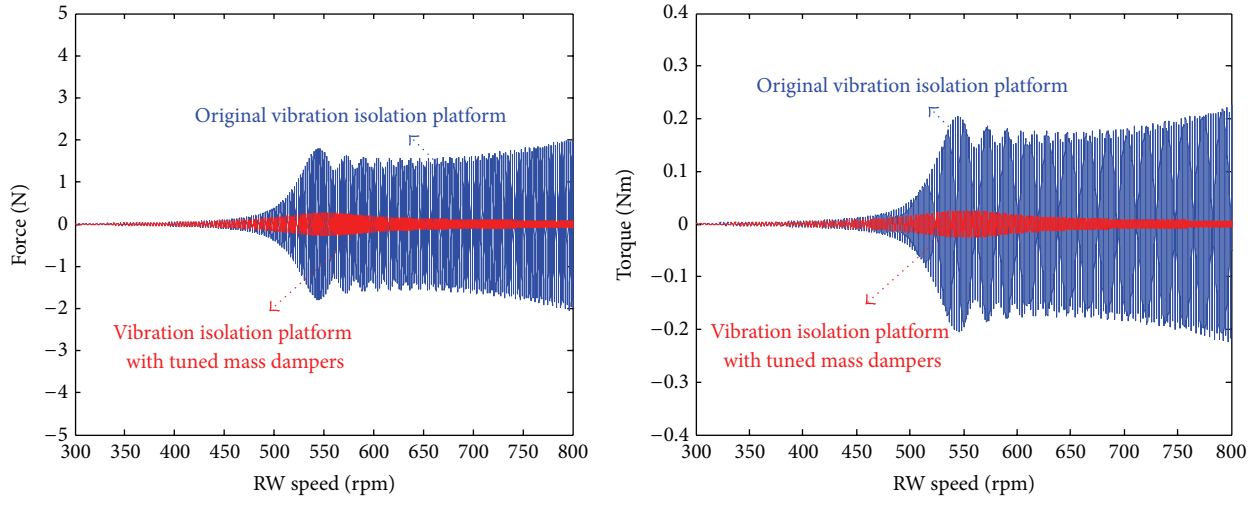

(a) (b)

Figure 14: Comparison curves of disturbances attenuation when the damping coefficient is 130 N·s/m.

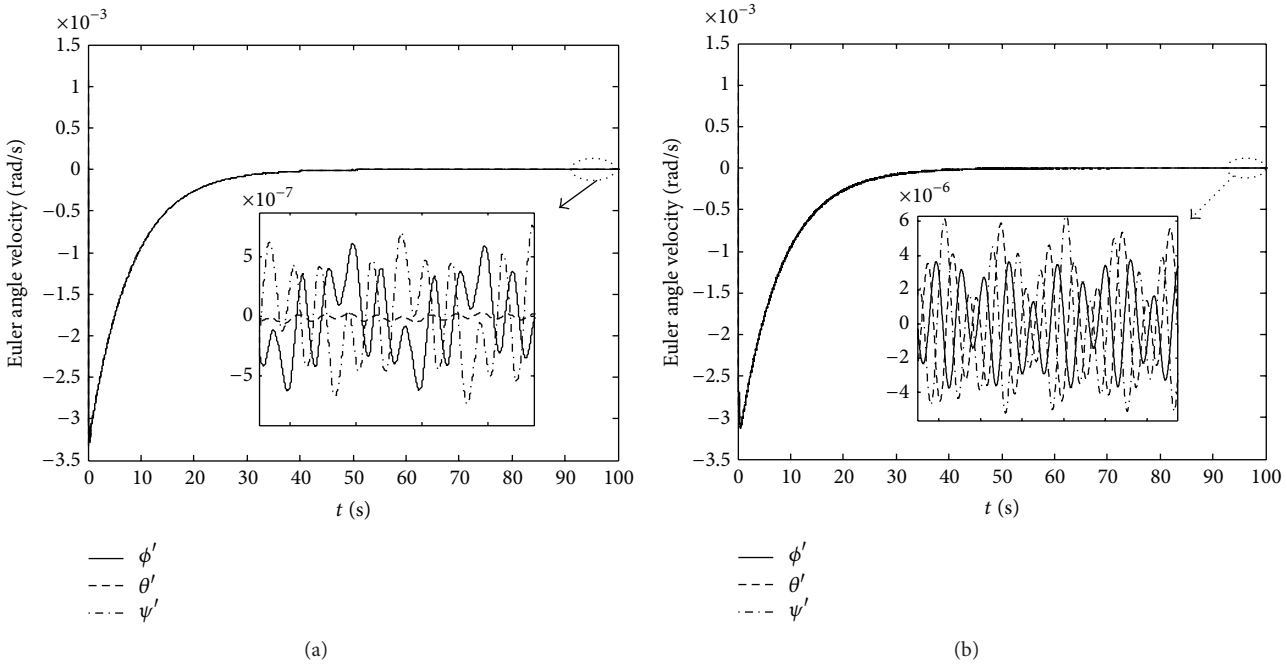

Figure 15: Attitude angular velocities of the satellite with and without the vibration isolation system.

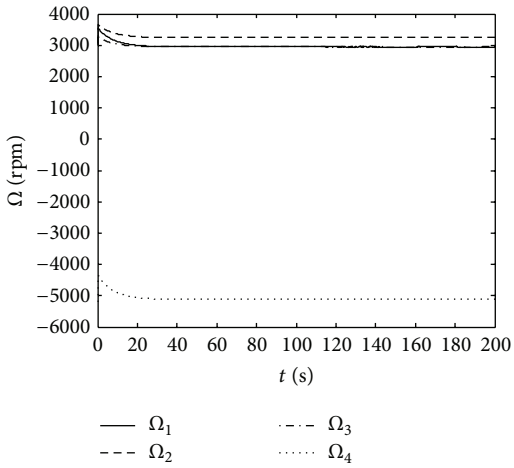

Figure 16: History of speeds of RWs with the vibration isolation system.

dampers is used, the maximal vibration amplitude is 5.2×10^{-7} rad/s, as shown in Figure 15(b). Under the disturbances of the RWs, the vibration isolation platform with tuned mass dampers is able to reduce the maximal vibration amplitude of the attitude angular velocities to 9% of that without any vibration isolation system. Therefore, the vibration isolation platform with tuned mass dampers can attenuate the disturbances to a considerable extent and can improve the attitude stability.

5. Conclusions

To isolate the vibration induced by the reaction wheel (RW), this study presented a new vibration isolation system which contains a multi-strut vibration isolation platform and multiple tuned mass dampers. This vibration isolation system can also be applied to isolating the vibration caused by other vibration sources, such as control moment gyroscopes and cryogenic cooler on satellites.

The dynamic model of the integrated satellite with this vibration isolation system and RWs by Newton-Euler Method has been derived. Compared to the dynamic models built by other researchers, this dynamic model not only takes the coupling effects between the RW and the vibration isolation platform into account but also considers the satellite bus movement and the dynamic characteristics of the RW. According to this dynamic model, jitter performance prediction of the spacecraft could be conveniently completed. Based on the assumption of small attitude angles, the transmissibility matrix of the vibration isolation platform with tuned mass dampers has been derived. It is indicated, from this transmissibility matrix, that the vibration isolation system presented in this paper has a good trade-off between the resonance amplitude and the high frequency attenuation. In addition, it is anticipated that the whole satellite dynamic model built and the calculation flow process of transmissibility matrix of this vibration isolation system will work for any other structure of vibration isolation systems. Finally, numerical simulations have been achieved, with results illustrating the effective attenuation of the RW disturbances by the vibration isolation system, and also validate the safety performance of it when the speed of the RW crosses the resonance frequency.

In further studies, for engineering realization of this new vibration isolation system, the influence of the installation position of this system, the offset of the center of mass of the vibration sources, and the dip angle of the payload platform on the performance of the attitude control of the spacecraft should be analyzed.

Acknowledgment

This work was supported by the Excellent Young Scholars Research Fund of Beijing Institute of Technology (Grant no. 2012YG0101).

References

[1] B. Agrawal, "Jitter control for imaging spacecraft," in *Proceedings of the 4th International Conference on Recent Advances in Space Technologies (RAST '09)*, pp. 615–620, Istanbul, Turkey, June 2009.

[2] T. T. Hyde, K. Q. Ha, J. D. Johnston, J. M. Howard, and G. E. Mosier, "Integrated modeling activities for the James Webb Space Telescope: optical jitter analysis," in *Optical, Infrared, and Millimeter Space Telecopes*, vol. 5487 of *Proceedings of SPIE*, pp. 588–599, gbr, June 2004.

[3] C. Blaurock, K. Liu, L. Dewell, and J. Alexander, "Passive isolator design for jitter reduction in the Terrestrial Planet Finder Coronagraph," in *Optical Modeling and Performance Predictions II*, vol. 5867-34, SPIE paper no. 5867-34, pp. 1–12, San Diego, Calif, USA, August 2005.

[4] R. Masterson, D. Miller, and R. Grogan, "Development of empirical and analytical reaction wheel disturbance models," in *Proceedings of the 40th AIAA/ASCE/AHS/ACS Structures, Structural Dynamics and Materials Conference*, April 1999.

[5] L. P. Davis and J. F. Wilson, "Hubble space telescope reaction wheel assembly vibration isolation system. Structural dynamics and control interaction of flexible structures," NASA Report N87-22702, 1986.

[6] J. C. Strain and S. Mittal, "Spacecraft redesign to reduce microphonic response of a VCO component," in *Proceedings of the 58th Shock and Vibration Symposium*, vol. 2, pp. 167–183, NASA. Marshall Space Flight Center, 1988.

[7] K. J. Pendergast and C. J. Schauwecker, "Use of a passive reaction wheel jitter isolation system to meet the Advanced X-ray Astrophysics Facility imaging performance requirements," in *Proceedings of the Conference on Space Telescopes and Instruments V. Part 1 (of 2)*, pp. 1078–1094, March 1998.

[8] A. J. Bronowicki, "Vibration isolator for large space telescopes," *Journal of Spacecraft and Rockets*, vol. 43, no. 1, pp. 45–53, 2006.

[9] D. Kamesh, R. Pandiyan, and A. Ghosal, "Modeling, design and analysis of low frequency platform for attenuating micro-vibration in spacecraft," *Journal of Sound and Vibration*, vol. 329, no. 17, pp. 3431–3450, 2010.

[10] R. Lourenco, *Design, Construction and Testing of an Adaptive Pendulum Tuned Mass Damper*, University of Waterloo, 2011.

[11] N. Hoang, Y. Fujino, and P. Warnitchai, "Optimal tuned mass damper for seismic applications and practical design formulas," *Engineering Structures*, vol. 29, no. 7, pp. 1548–1560, 2007.

[12] Q. Li, J. Fan, J. Nie, Q. Li, and Y. Chen, "Crowd-induced random vibration of footbridge and vibration control using multiple tuned mass dampers," *Journal of Sound and Vibration*, vol. 329, no. 19, pp. 4068–4092, 2010.

[13] Y. Q. Guo and W. Q. Chen, "Dynamic analysis of space structures with multiple tuned mass dampers," *Engineering Structures*, vol. 29, no. 12, pp. 3390–3403, 2007.

[14] I. Basdogan, R. Grogan, A. Kissil, N. Sigrist, and L. Sievers, "Preliminary optical performance analysis of the space interferometer mission using an integrated modeling methodology," in *Proceedings of the Control of Vibration and Noise-New Millennium: International Mechanical Engineering Congress & Exposition 6th Biennial Symposium on Active Control of Vibration and Noise*, Orlando, Fla, USA, November 2000.

[15] L. Dewell, N. Pedreiro, C. Blaurock, K. Liu, J. Alexander, and M. Levine, "Precision telescope pointing and spacecraft vibration isolation for the terrestrial planet finder coronagraph," in *Proceedings of the UV/Optical/IR Space Telescopes: Innovative Technologies and Concepts II*, pp. 1–14, San Diego, Calif, USA, August 2005.

[16] S. E. Miller, P. Kirchman, and J. Sudey, "Reaction wheel operational impacts on the GOES-N jitter environment," in *Proceedings of the AIAA Guidance, Navigation, and Control Conference*, pp. 3642–3653, Hilton Head Island, SC, USA, August 2007.

[17] K. Liu, P. Maghami, and C. Blaurock, "Reaction wheel disturbance modeling, jitter analysis, and validation tests for Solar Dynamics Observatory," in *Proceedings of the AIAA Guidance, Navigation and Control Conference and Exhibit*, Honolulu, Hawaii, August 2008.

[18] M. Luis, T. Frank, A. Satya, S. Victor, and H. Tupper, "Line of sight stabilization for the James Webb Space Telescope," *Advances in the Astronautical Sciences*, vol. 121, pp. 17–30, 2005.

[19] B. Dasgupta and T. S. Mruthyunjaya, "A Newton-Euler formulation for the inverse dynamics of the Stewart platform manipulator," *Mechanism and Machine Theory*, vol. 33, no. 8, pp. 1135–1152, 1998, International Conference on Advances in Mechanical Engineering (ICAME) (Bangalore, 1995).

[20] Z. Yao, Z. Jingrui, and X. Shijie, "Parameters design of vibration isolation platform for control moment gyroscopes," *Acta Astronautica*, vol. 81, no. 2, pp. 645–659, 2012.

[21] F. Zhang, G. Duan, and M. Hou, "Integrated relative position and attitude control of spacecraft in proximity operation missions with control saturation," *International Journal of Innovative Computing, Information and Control*, vol. 8, no. 5B, pp. 3537–3551, 2012.

[22] Y. Cheng, B. Jiang, Y. Fu, and Z. Gao, "Robust observer based reliable control for satellite attitude control systems with sensor faults," *International Journal of Innovative Computing, Information and Control*, vol. 7, no. 7B, pp. 4149–4160, 2011.

[23] Y. Zhang, J.-R. Zhang, and S.-J. Xu, "Influence of flexible solar arrays on vibration isolation platform of control moment gyroscopes," *Acta Mechanica Sinica*, vol. 28, no. 5, pp. 1479–1487, 2012.